Electrokinetics of Diffuse Soft Interfaces. 1. Limit of Low Donnan Potentials

ARTICLE *in* LANGMUIR · DECEMBER 2004

Impact Factor: 4.46 · DOI: 10.1021/la0400508 · Source: PubMed

2 AUTHORS, INCLUDING:

Jerome F.L. Duval

French National Centre for Scientific Research

111 PUBLICATIONS **1,941** CITATIONS

Electrokinetics of Diffuse Soft Interfaces. 1. Limit of Low Donnan Potentials

Jérôme F. L. Duval* and Herman P. van Leeuwen

Department of Physical Chemistry and Colloid Science, Dreijenplein 6, 6703 HB Wageningen, The Netherlands

Received March 22, 2004. In Final Form: August 25, 2004

The current theoretical approaches to electrokinetics of gels or polyelectrolyte layers are based on the assumption that the position of the very interface between the aqueous medium and the gel phase is well defined. Within this assumption, spatial profiles for the volume fraction of polymer segments (ϕ), the density of fixed charges in the porous layer (ρ_{fix}), and the coefficient modeling the friction to hydrodynamic flow (k) follow a step-function. In reality, the "fuzzy" nature of the charged soft layer is intrinsically incompatible with the concept of a *sharp interface* and therefore necessarily calls for more detailed spatial representations for ϕ, ρ_{fix}, and k. In this paper, the notion of *diffuse interface* is introduced. For the sake of illustration, linear spatial distributions for ϕ and ρ_{fix} are considered in the *interfacial zone* between the bulk of the porous charged layer and the bulk electrolyte solution. The corresponding distribution for k is inferred from the Brinkman equation, which for low ϕ reduces to Stokes' equation. Linear electrostatics, hydrodynamics, and electroosmosis issues are analytically solved within the context of streaming current and streaming potential of charged surface layers in a thin-layer cell. The hydrodynamic analysis clearly demonstrates the physical incorrectness of the concept of a discrete slip plane for diffuse interfaces. For moderate to low electrolyte concentrations and nanoscale spatial transition of ϕ from zero (bulk electrolyte) to ϕ_0 (bulk gel), the electrokinetic properties of the soft layer as predicted by the theory considerably deviate from those calculated on the basis of the discontinuous approximation by Ohshima.

1. Introduction

In the past decade, much attention has been devoted to the development of theories describing electrokinetic features of "soft" or "hairy" spherical particles[1−9] (see ref 9 for further references). Such particles usually consist of a hard core covered by an adsorbed polyelectrolyte layer characterized by a three-dimensional spatial distribution of hydrodynamically stagnant, ionogenic groups. The resulting charged layer is sometimes called the "charged surface layer", even if the qualification "surface" loses its well-defined meaning here. In the complete absence of a particle core, the soft particle becomes a spherical polyelectrolyte (porous sphere).[10−13] Gel-like surfaces also fall in the category of soft surfaces in the sense that they consist of a defined network of polymer segments (of given density of charged groups) which is penetrable for ions or small colloids.[14−16] It has long been recognized that the electrophoretic behavior of soft particles and the electrokinetics (streaming potential, streaming current) of gel layers (GLs) substantially deviate from those of hard (i.e., rigid) particles and hard flat surfaces, respectively. The reasons for this are essentially electrostatic and hydrodynamic in nature. In the interphasial region, the distribution of fixed charged groups in the ion-permeable layer takes place within distances comparable to, if not larger than, the Debye length, thus considerably modifying the electric potential distribution as derived from hard-surface models.[17] Also, electroosmotic flow[1,18,19] and/or penetration of hydrodynamic flow inside the layer[9] may lead to orders of magnitude discrepancy between the observed electrokinetic response and that expected on the basis of the classical Helmholtz−Smoluchowski approach.

The currently available theories have a number of fundamental aspects in common regarding the electric and hydrodynamic modeling of the GL. As far as the electrostatics is concerned, the concept of Donnan potential, or for that matter Donnan equilibrium, has gained some consensus.[18] This concept is analogous to that of equilibrium potential set up between two solutions of different ionic compositions separated by an ion-exchange membrane. The Donnan potential depends on the concentration of ions and density distribution of fixed charged groups (ρ_{fix}) in the GL.[20] For the sake of simplicity, the distribution of these groups is commonly considered *uniform*, that is, isotropic in all spatial dimensions. The hydrodynamics is classically tackled using the macroscopic Debye−Bueche[21] or microscopic Kirkwood−Riseman[22]

* To whom correspondence should be addressed. E-mail: jerome.duval@wur.nl. Tel: 00 31 317 484 960. Fax: 31 (0)317 483 777.

(1) Donath, E.; Pastuschenko, V. *Bioelectrochem. Bioenerg.* **1979**, *6*, 543.
(2) Jones, I. S. *J. Colloid Interface Sci.* **1979**, *68*, 451.
(3) Wunderlich, R. W. *J. Colloid Interface Sci.* **1982**, *88*, 385.
(4) Ohshima, H.; Ohki, S. *Biophys. J.* **1985**, *47*, 673.
(5) Ohshima, H.; Kondo, T. *Colloid Polym. Sci.* **1986**, *264*, 1080.
(6) Ohshima, H.; Kondo, T. *J. Colloid Interface Sci.* **1987**, *116*, 305; **1989**, *130*, 281; **1990**, *135*, 443.
(7) Ohshima, H.; Kondo, T. *J. Theor. Biol.* **1987**, *124,* 191.
(8) Ohshima, H. *J. Colloid Interface Sci.* **1994**, *163*, 474.
(9) Ohshima, H. *Adv. Colloid Interface Sci.* **1995**, *62*, 189.
(10) Hermans, J. J. *J. Polym. Sci.* **1955**, *18*, 527.
(11) Hermans, J. J.; Fujita, H. *K. Ned. Akad. Wet. Proc.* **1955**, *B58*, 182.
(12) Overbeek, J. Th. G.; Stigter, D. *Recl. Trav. Chim.* **1956**, *75*, 543.
(13) Imai, N.; Iwasa, K. *Isr. J. Chem.* **1973**, *11*, 223.
(14) Starov, V.; Solomentsev, Y. E. *J. Colloid Interface Sci.* **1993**, *158*, 159.
(15) Starov, V.; Solomentsev, Y. E. *J. Colloid Interface Sci.* **1993**, *158*, 166.
(16) Donath, E.; Voigt, A. *J. Colloid Interface Sci.* **1986**, *109*, 122.
(17) Hunter, R. J. *Zeta-potential in colloid science. Principles and applications*; Academic Press: New York, 1981.
(18) Donath, E.; Pastuschenko, V. *Bioelectrochem. Bioenerg.* **1980**, *7*, 31.
(19) Pastuschenko, V.; Donath, E. *Stud. Biophys.* (*Berlin*) **1976**, *56*, 7.
(20) Ohshima, H.; Kondo, T. *Biophys. Chem.* **1990**, *38*, 117.
(21) Debye, P.; Bueche, A. *J. Chem. Phys.* **1948**, *16*, 573.
(22) Kirkwood, J.; Riseman, J. *J. Chem. Phys.* **1948**, *16*, 565.

10.1021/la0400508 CCC: $27.50
Published on Web 10/15/2004

theories. These models account for the frictional properties of dilute polymer solutions, as encountered in gel layers of low material density (ϕ). Despite their different levels of approach, the physical ideas underlying these two theories are similar, as later shown by Felderhof and Deutch.[23] Roughly speaking, the polymer segments in the GL are regarded as *uniformly distributed* resistance centers which exert frictional forces on the liquid flowing in the layer. Differences between existing theories refer to their degree of mathematical sophistication (linearization[1,2,16,18,19] or not[9,14,15,16] of the Poisson−Boltzmann equation), to their ability to generalize electrokinetic behavior of various systems (spherical polyelectrolytes, soft particles, rigid particles, gels, or all types of surfaces[8,9]), to their accounting for specific interactions between electrolyte ions and polymer segments,[15] or to the modeling of the dissociation properties of the ionogenic groups inside the GL.[16,24] The assumption of a uniform spatial distribution for ϕ, ρ_{fix}, and the friction coefficient k in the GL is basically motivated by the simplicity of the mathematics required to obtain the resulting solutions of the Poisson−Boltzmann and Navier−Stokes equations. Although this theoretical approach has played its role in the progress of our understanding of the peculiar electrokinetic behavior of charged structured layers, it is an abstraction from reality as suggested by recent molecular dynamics (MD) simulations.[25] The results of these MD studies motivate the quest for a better modeling of interfaces at soft structures, as justified by electrokinetic surveys which fail to match theoretical predictions for low electrolyte concentrations.[26−29] In ref 25, Lyklema et al. mimic the interactions between ions, water molecules, and the wall of a dense material via Lennard-Jones type potential profiles and apply a force tangential to the (rigid) surface. Density distributions of ions and water molecules are canonically time-averaged over a long time interval, their trajectories followed in the vicinity of the surface and the fluid viscosity determined from the time correlation of the pressure tensor as a function of distance from the wall. In the absence of a tangential force, the analysis clearly shows the (already recognized) presence of *a stacking layer* with a thickness of two to three solvent molecules. This layer roughly corresponds to the Stern layer, and the interesting feature is that *no discrete transition* between the stacking layer and the bulk solution is observed. When applying a tangential force, the dynamic nature of the Stern layer is highlighted: from the trajectories of ions and solvent molecules, *anisotropy* of the fluid viscosity emerges. The viscosities parallel to and in the vicinity of the surface are the same as in the bulk or higher by a factor of 2, and the viscosity perpendicular to the surface is 4−5 times higher than in the bulk. This results in the phenomenological observation of a *stagnant layer* close to the surface, stagnant meaning hydrodynamically immobile. The qualification "stagnant" only pertains to the water molecules since the tangential mobility of the ions in the Stern layer is practically equal to that in the bulk. Viscous flow of water is a cooperative process limited by the resistance of the solvent molecules to leave or enter the Stern layer, whereas ionic transport within the stagnant layer is more an individual phenomenon. GLs effectively behave like stagnant layers. The friction exerted by the polymer segments on the water molecules is responsible for fluid stagnancy, but transport of ions and other low molar mass solutes is virtually unimpeded. The fundamental difference with rigid materials is that friction coefficients in GLs as commonly reported in the literature give rise to nonzero fluid velocities (see section 3) deep inside the layer. Consequently, for a GL the concept of a slip plane (which corresponds to the position where the fluid velocity drops to zero) or a zeta-potential is undefined and thus nonapplicable. Moreover, the steric and electrostatic interactions between (charged) polymers, solvent molecules, and ions that are unevenly distributed across the electrolyte/GL interphase necessarily result in a *gradual transition* of the volume fraction of polymer segments from a constant value (bulk gel) to zero (bulk solution). In other words, the stagnant layer, which for a GL may even exceed the micrometer scale,[28] is inhomogeneous in space and, therefore, contrary to the case of hard surfaces, there is no practical way to locate a plane marking the transition between the bulk GL and the bulk electrolyte solution. It is recalled here that the fibers or polymer segments constituting the layer are flexible and their characteristic size and spatial arrangements strongly depend on their neighboring environment and, in particular, are mediated by the local distributions of electrolyte ions. In polymer chemistry, self-consistent-field calculations[30] (see ref 30 for further references), as based on the Scheutjens−Fleer theory,[31] and molecular dynamic simulations are commonly used to determine the inhomogeneous spatial distribution of adsorbed polymers at a given surface.[32,33] Experimental evidence, provided by atomic force microscopy or other imaging and spectroscopic techniques, also confirms the existence of such interfacial inhomogeneities. All these elements motivate the abandoning of step-function type modeling for an interface between a soft structured layer and an electrolyte solution. In the following, we shall rather use the term *diffuse interface*, stressing that continuous spatial profiles for ϕ, ρ_{fix}, and k across the interphasial region are explicitly taken into account. Though the necessity of considering a gradual transition of ρ_{fix} has already been recognized by a few authors,[20,34] the consequences of electrostatic anisotropy for the hydrodynamics and subsequently for the electrokinetics have only been very scarcely touched upon. Here we shall present a hydrodynamically and electrostatically rigorous analysis of the problem, starting from given profiles of ϕ and ρ_{fix}. The ensuing electrokinetic properties will be compared with those derived from the less sophisticated approaches developed by Ohshima for the electrophoresis of soft particles[9] or by Donath and Voigt[16] and Starov and Solomentsev[14,15] for the streaming potential analyses of structured layers. These models assume a uniform polymer segment distribution and are based on the simplifying assumption that a softness parameter λ is independent of position (see the next section).

(23) Felderhof, B.; Deutch, J. *J. Chem. Phys.* **1975**, *62*, 2391.
(24) Donath, E.; Budde, A.; Knippel, E.; Bäumler, H. *Langmuir* **1996**, *12*, 4832.
(25) Lyklema, J.; van Leeuwen, H. P.; Minor, M. *Adv. Colloid Interface Sci.* **1999**, *83*, 33.
(26) Makino, K.; Yamamoto, S.; Fujimoto, K.; Kawaguchi, H.; Ohshima, H. *J. Colloid Interface Sci.* **1994**, *166*, 251.
(27) Ohshima, H.; Makino, K.; Kato, T.; Fujimoto, K.; Kondo, T.; Kawaguchi, H. *J. Colloid Interface Sci.* **1993**, *159*, 512.
(28) Yezek, L.; Duval, J. F. L.; van Leeuwen, H. P. *Langmuir*, to be submitted.
(29) Garcia-Salinas, M. J.; Romero-Cano, M. S.; de Las Nieves, F. J. *J. Colloid Interface Sci.* **2001**, *241*, 280.
(30) Van Male, J. Self-consistent-field theory for chain molecules: extensions, computational aspects, and applications. Ph.D. Thesis, Wageningen University, Wageningen, The Netherlands, 2003.
(31) Scheutjens, J. M. H. M.; Fleer, G. J. *J. Phys. Chem.* **1979**, *83*, 1619.
(32) Van der Gucht, J.; Besseling, N. A. M. *Phys. Rev. E* **2002**, *56*, 51801.
(33) Zhulina, E. B.; Klein Wolterink, J.; Borisov, O. V. *Macromolecules* **2000**, *33*, 4945.
(34) Ohshima, H. *J. Colloid Interface Sci.* **1997**, *185*, 269.

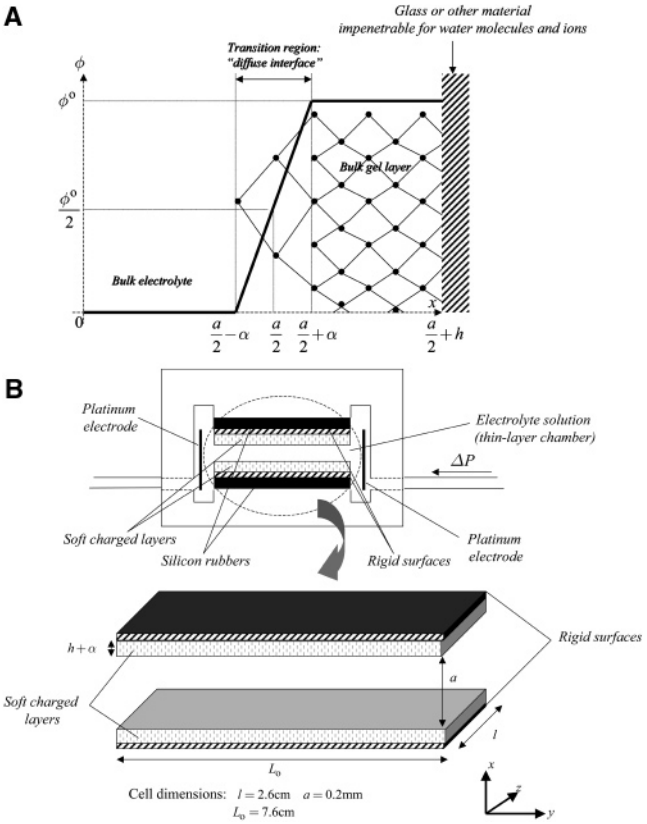

Figure 1. Schematic representation of (A) the spatial modeling of the diffuse interface between an electrolyte solution and a structured charged layer and (B) the electrokinetic cell used for the streaming potential and streaming current measurement. The position $x = 0$ corresponds to the middle of the cell.

2. Modeling of the Diffuse Gel/Solution Interface

Though differences in ion valencies may be easily accounted for, we consider here an ion-penetrable structure immersed in a 1:1 electrolyte of bulk concentration n_∞. For the sake of illustration, Figure 1A represents a soft structure as a network of cross-linked polymer segments (gel structure) but it could also consist of irreversibly attached polymers, as in the case of most biological surfaces (polyelectrolyte layers), without loss of generality for the theory we propose. The so-formed layer may be realized via different processes (chemisorption or physisorption on rigid surfaces) that we shall not detail here. A flat and smooth surface represents the inner boundary of the layer and is considered to be uncharged. We consider the electrokinetic properties of the soft layer/solution interface in a parallelepipedic cell of which the experimental arrangement and the characteristic sizes (width l, length L_o, and height a) are given in Figure 1B.[35] The Cartesian coordinate system chosen is also represented. A pressure gradient $\Delta P/L_o$ is applied along the thin-layer chamber in the cell (y-axis). Two electrodes placed at the extremities of the chamber allow measurement of the current or lateral potential difference produced by the flow (streaming current or streaming potential, respectively).

It is merely assumed that there is a given spatial profile for the density of charged polymer segments $\phi(x)$ within the soft layer, x being the dimension perpendicular to the layers of interest. Rigorous determination of the distribution $\phi(x)$ requires knowledge of the type of interactions existing within the system (polymer segments−solvent molecules−electrolyte ions) and knowledge of the details concerning the preparation of the soft structure and subsequent grafting on the boundary surface. As a first-order approach, we shall choose in the following a linear distribution for ϕ, valid for the nanometer-scale interfacial region (see Figure 1). Hence, we write $\phi(x)$ in the form

$$\phi(x) = \begin{cases} 0 & \text{for } 0 \le x \le a/2 - \alpha \\ \dfrac{\phi_o}{2}\left(1 + \dfrac{x - a/2}{\alpha}\right) & \text{for } a/2 - \alpha \le x \le a/2 + \alpha \\ \phi_o & \text{for } a/2 + \alpha \le x \le a/2 + h \end{cases} \quad (1a-c)$$

with ϕ_o the density of polymer segments in the bulk of the layer. α characterizes the typical thickness of the interfacial region (diffuse interface), and $h - \alpha$ that of the bulk layer ($h \gg \alpha$). Assuming that the distribution of charged sites along the polymer segments is uniform, the spatial profile for the fixed charge density ρ_{fix} follows that of ϕ. $\rho_{fix}(x)$ is then given by eq 1 after replacing ϕ_o by ρ_o, the bulk density of fixed charged groups in the layer. To obtain the spatial distribution of k, the coefficient of friction exerted by the polymer segments on the water molecules, we choose the Brinkman equation,[36] which relates k to ϕ by considering the flux of fluid across a group of spheres of radius R, the so-called resistance centers:

$$\lambda(x) = \left\{\frac{R^2}{18}\left[3 + \frac{4}{\phi(x)} - 3\left(\frac{8}{\phi(x)} - 3\right)^{1/2}\right]\right\}^{-1/2} \quad (2)$$

which is valid for $\phi < 0.6$. The parameter $\lambda = (k/\eta_w)^{1/2}$ (with η_w the dynamic viscosity of water) depends on the position x and is a measure of the softness of the layer: $\lambda^{-1}(x)$ has the dimension of a length and characterizes the degree of penetration of the fluid into the infinitesimal slice of charged layer located at the position x. The fundamental difference with the studies reported in ref 9 is that now the softness parameter is a function of the position, as a consequence of the gradual distribution of polymer segments across the diffuse interface. A number of empirical expressions $\lambda(\phi)$ confirm the validity of eq 2.[37-39] One may show that eq 2 can be transformed as follows:

$$\lambda(x) = \tilde{\lambda} \sum_{n=1}^{\infty} \sigma_n [\phi(x)]^{n/2} \quad (3)$$

with $\tilde{\lambda} = 3(\sqrt{2})/R$ and σ_n the coefficients in the Taylor expansion of eq 2 with respect to the variable $\phi^{1/2}$. For low volume fractions, only the first term is significant and eq 3 reduces to Stokes' equation which predicts a linear dependence of λ and k on $\phi^{1/2}$ and ϕ, respectively. In the following, we shall adopt this relationship which is justified for the usual water contents of gels or polyelectrolyte layers commonly reported in the literature ($\phi < 0.05$). Within this framework, $k(x)$ may be represented by a linear profile as given in eq 1, after replacing ϕ_o by k_o, the friction coefficient in the bulk layer (the corresponding softness parameter is given by $\lambda_o = (k_o/\eta_w)^{1/2}$). In a future communication, the electrokinetics for more dense charged layers will be addressed.

(35) Van Wagenen, R. A.; Andrade, J. D. *J. Colloid Interface Sci.* **1980**, *76* (2), 305.

(36) Brinkman, H. C. *Research* **1949**, *2*, 190.

(37) Carman, P. C. *Trans. Inst. Chem. Eng. London* **1937**, *15*, 150.

(38) Cohen-Stuart, M. A.; Waajen, F. H. W. H., Cosgrove, T.; Vincent, B.; Crowley, T. L. *Macromolecules* **1984**, *17*, 1825.

(39) Fernandez-Nieves, A.; Fernandez-Barbero, A.; de las Nieves, F. J.; Vincent, B. *J. Phys.: Condens. Matter* **2000**, *12*, 3605.

3. Hydrodynamics: Determination of the Velocity Profile

Under the conditions outlined in the previous section, the direction of the bulk stream of flow is parallel to the surface and the steady-state velocity profile in the channel is represented by $v(x)$, as defined by the pertaining Navier–Stokes equation. The problem is symmetric with respect to $x = 0$ (the center of the cell), and therefore the analysis will be restricted to the interval $0 \le x \le a/2 + h$. For $0 \le x \le a/2 - \alpha$ (outside the gel layer), $v(x)$ is simply given by

$$\frac{d^2v(x)}{dx^2} = -\frac{\Delta P}{\eta_w L_o} \tag{4}$$

In the region corresponding to a gradual transition of the friction coefficient ($a/2 - \alpha \le x \le a/2 + \alpha$), we have

$$\frac{d^2v(x)}{dx^2} - \frac{\lambda_o^{-2}}{2}\left(1 + \frac{x - a/2}{\alpha}\right)v(x) = -\frac{\Delta P}{\eta_w L_o} \tag{5}$$

where it is assumed that the friction exerted by the gel fibers on the water molecules remains proportional to the velocity; that is, hydrodynamic interactions are not taken into account. Within the framework of this assumption, which holds for the laminar flow regime (Reynolds number $Re < 2500$), $v(x)$ inside the gel layer ($a/2 + \alpha \le x \le a/2 + h$) is governed by

$$\frac{d^2v(x)}{dx^2} - \lambda_o^{-2}v(x) = -\frac{\Delta P}{\eta_w L_o} \tag{6}$$

Equations 4–6 hold for steady-state conditions (no transient taken into account). The boundary conditions associated with the linear differential equations of the second order, eqs 4–6, are given by continuity of the velocity profiles at $x = a/2 - \alpha$, $a/2 + \alpha$,

$$v(x)|_{(a/2-\alpha)^-} = v(x)|_{(a/2-\alpha)^+}$$

$$\frac{dv(x)}{dx}|_{(a/2-\alpha)^-} = \frac{dv(x)}{dx}|_{(a/2-\alpha)^+} \tag{7a,b}$$

$$v(x)|_{(a/2+\alpha)^-} = v(x)|_{(a/2+\alpha)^+}$$

$$\frac{dv(x)}{dx}|_{(a/2+\alpha)^-} = \frac{dv(x)}{dx}|_{(a/2+\alpha)^+} \tag{8a,b}$$

by stagnancy at $a/2 + h$,

$$v(x)|_{(a/2+h)} = 0 \tag{9}$$

and symmetry with respect to $x = 0$

$$\frac{dv(x)}{dx}|_0 = 0 \tag{10}$$

The general solution of eq 4 is simply given by

$$0 \le x \le a/2 - \alpha: \quad v(x) = -\frac{\Delta P}{2\eta_w L_o}x^2 + C_1x + C_2 \tag{11}$$

where C_1 and C_2 are constants (to be specified below). Equation 5 can be solved via series expansion,

$$a/2 - \alpha \le x \le a/2 + \alpha: \quad v(x) = \sum_{n=1}^{\infty} v_n[u(x)]^n \tag{12}$$

where v_n are the coefficients in the polynomial development of $v(x)$ with respect to the dimensionless spatial variable $u(x)$ defined by

$$u(x) = 1 + \frac{x - a/2}{\alpha} \tag{13}$$

After introducing eq 12 in eq 5 and collecting the terms of the order $O(u^n)$, one obtains

$$\left(2v_2 + \frac{\Delta P\alpha^2}{\eta_w L_o}\right) + \sum_{n=3}^{\infty}[n(n-1)v_n - \theta v_{n-3}][u(x)]^{n-2} = 0 \tag{14}$$

where θ is the dimensionless parameter

$$\theta = \frac{(\alpha\lambda_o)^2}{2} \tag{15}$$

In order for eq 14 to hold for all x, each separate term must be zero. Therefore, one infers

$$v_2 = -\frac{\Delta P\alpha^2}{2\eta_w L_o} \tag{16}$$

$$n \ge 3: \quad n(n-1)v_n - \theta v_{n-3} = 0 \tag{17}$$

Starting from the recursive formula 17, one shows that $v(x)$ is of the form

$$v(x) = v_0 + v_1u(x) + v_2[u(x)]^2 + \sum_{j=0}^{2}\sum_{n=1}^{\infty} v_{3n+j}[u(x)]^{3n+j} \tag{18}$$

with the terms $(v_{3n+j})_{n\ge1,0\le j\le2}$ given by

$$(v_{3n+j})_{n\ge1,0\le j\le2} = \theta^n\frac{j!}{(3n+j)!}f(n,j)v_j \tag{19}$$

and the function f defined by

$$f(n,j) = \prod_{p=0}^{n-1}(3p + j + 1) \tag{20}$$

Integration of differential eq 6 is straightforward:

$a/2 + \alpha \le x \le a/2 + h$:

$$v(x) = \frac{\Delta P}{\eta_w L_o \lambda_o^{-2}} + C_3\exp\left[\frac{-x + (a/2 + \alpha)}{\lambda_o^{-1}}\right] + C_4\exp\left[\frac{x - (a/2 + h)}{\lambda_o^{-1}}\right] \tag{21}$$

with C_3 and C_4 constants. To explicitly compute the spatial distribution $v(x)$, the constants $(C_i)_{1\le i\le4}$ and the terms $(v_i)_{i=0,1}$ remain to be determined. The 6 linearly independent equations required for that purpose are provided by the boundary conditions 7–10. Equation 10 immediately yields $C_1 = 0$, and after rearrangement, eqs 7–9 become

$$C_2 = v_0 + \frac{\Delta P}{2\eta_w L_o}\left(\frac{a}{2} - \alpha\right)^2 \tag{22}$$

$$v_1 = -\frac{\Delta P\alpha}{\eta_w L_o}\left(\frac{a}{2} - \alpha\right) \tag{23}$$

$$\frac{\Delta P}{\eta_w L_o {\lambda_o}^2} + C_3 + C_4 \exp[\lambda_o(\alpha - h)] - \sum_{j=0}^{2} 2^j v_j \left(1 + \sum_{n=1}^{\infty} \theta^n \frac{2^{3n}\, j!}{(3n+j)!} f(n,j)\right) = 0 \quad (24)$$

$$(2\theta)^{1/2}(C_4 \exp[\lambda_o(\alpha - h)] - C_3) - \sum_{j=0}^{2} v_j \left(j^2 + \sum_{n=1}^{\infty} \theta^n \frac{2^{3n+j-1}\, j!}{(3n+j-1)!} f(n,j)\right) = 0 \quad (25)$$

$$C_4 = -\left(\frac{\Delta P}{\eta_w L_o {\lambda_o}^2} + C_3 \exp[\lambda_o(\alpha - h)]\right) \quad (26)$$

After replacing C_4 in eqs 24−25 by the expression given in eq 26, one obtains

$$C_3 = \frac{1}{\mathcal{J}\{1 - \exp[2\lambda_o(\alpha - h)]\} + \mathcal{R}(2\theta)^{1/2}\{1 + \exp[2\lambda_o(\alpha - h)]\}} \times \left[\mathcal{J}\sum_{j=1}^{2} 2^j v_j \left(1 + \sum_{n=1}^{\infty} \theta^n \frac{2^{3n}\, j!}{(3n+j)!} f(n,j)\right) - \mathcal{R}\sum_{j=1}^{2} v_j \left(j^2 + \sum_{n=1}^{\infty} \theta^n \frac{2^{3n+j-1}\, j!}{(3n+j-1)!} f(n,j)\right) + \frac{\Delta P}{\eta_w L_o {\lambda_o}^2}\{\mathcal{J}\{\exp[\lambda_o(\alpha - h)] - 1\} - \mathcal{R}(2\theta)^{1/2} \exp[\lambda_o(\alpha - h)]\}\right] \quad (27)$$

$$v_0 = \frac{-1}{\mathcal{J}\{1 - \exp[2\lambda_o(\alpha - h)]\} + \mathcal{R}(2\theta)^{1/2}\{1 + \exp[2\lambda_o(\alpha - h)]\}} \times \left[(1 + \exp[2\lambda_o(\alpha - h)])(2\theta)^{1/2}\sum_{j=1}^{2} 2^j v_j \left(1 + \sum_{n=1}^{\infty} \theta^n \frac{2^{3n}\, j!}{(3n+j)!} f(n,j)\right) + (1 - \exp[2\lambda_o(\alpha - h)]) \sum_{j=1}^{2} v_j \left(j^2 + \sum_{n=1}^{\infty} \theta^n \frac{2^{3n+j-1}\, j!}{(3n+j-1)!} f(n,j)\right) - \frac{\Delta P}{\eta_w L_o {\lambda_o}^2}(2\theta)^{1/2}\{(1 - \exp[\lambda_o(\alpha - h)])(1 + \exp[2\lambda_o(\alpha - h)]) - \exp[\lambda_o(\alpha - h)](1 - \exp[2\lambda_o(\alpha - h)])\}\right] \quad (28)$$

with $\mathcal{J}$ and $\mathcal{R}$ defined by

$$\mathcal{J} = \sum_{n=1}^{\infty} \theta^n \frac{2^{3n-1}}{(3n-1)!} f(n, 0) \quad (29)$$

$$\mathcal{R} = 1 + \sum_{n=1}^{\infty} \theta^n \frac{2^{3n}}{(3n)!} f(n, 0) \quad (30)$$

The constants C_2 and C_4 follow directly from eqs 22 and 26, respectively. The terms v_1 and v_2 in the Taylor expansion of v are given by eqs 23 and 16, respectively.

At this stage of the analysis, the distribution $v(x)$ is fully determined. In Figure 2, characteristic velocity profiles $v(x)$ in the thin-layer chamber of the electrokinetic cell are shown for different values of the hydrodynamic penetration length λ_o^{-1}. The two limits $\lambda_o^{-1} \to 0$ and $\lambda_o^{-1} \to \infty$ refer to the cases of rigid surfaces positioned at $x = \pm a/2$ (no flow penetration in the GLs) and at $x = \pm(a/2 + h)$ (no friction exerted in the "GLs"), respectively. The hydrodynamics for these limiting cases is simply described by a parabolic Poiseuille profile for a fluid confined in channels of thickness a and $a + 2h$, respectively. For intermediate values of λ_o^{-1}, the flow velocity in the GLs increases with decreasing friction (panel A). Also, the maximum velocity, reached at $x = 0$, is influenced by the presence of the GLs ($v(x = 0) = C_2$ increases with λ_o^{-1} and decreases with α). To clearly show the velocity distribution in the region corresponding to the diffuse interface ($a/2 - \alpha \le x \le a/2 + \alpha$), profiles $v(x)$ are given in Figure 2B for $h/\alpha = 6$ and hydrodynamic penetration lengths of nanometer scale, which corresponds to practical values of λ_o^{-1}.[26−29] The details of the flow distribution within the diffuse interface are obviously of importance for the electrokinetics of GLs for which $\kappa\alpha \approx 1$ (see section 5). In this situation, which is consistent with the linear gradient chosen for $k(x)$, the local concentrations of counterions in the diffuse interface are significant (see section 4). Besides,

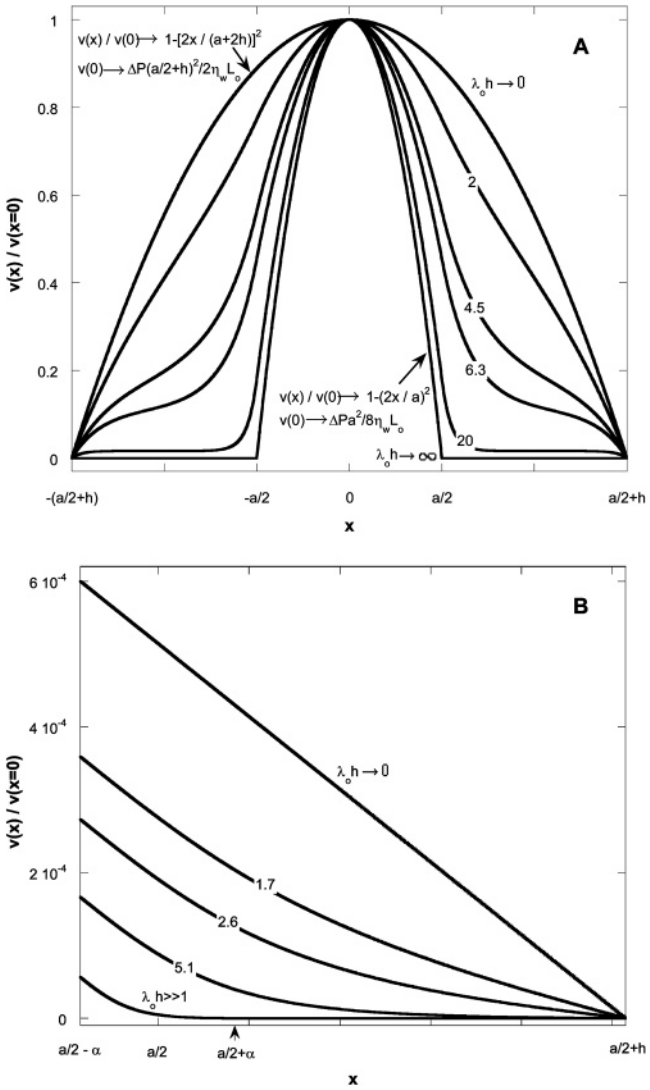

Figure 2. (Panel A) Normalized flow velocity profile in the thin-layer chamber as a function of the dimensionless softness parameter $\lambda_o h$ (indicated). In the calculations, $h = a$, $\kappa\alpha = 1$, and $c_\infty = 5$ mM. (Panel B) Representation of the normalized flow velocity profile in the diffuse interface and bulk gel layer (GL) for $h = 6\alpha$ and various $\lambda_o h$ as indicated. Other model parameters are as in panel A.

the fluid velocity remains small as compared to that in the bulk solution ($v(x)/v(0) < 0.1$ %) but there is still no unambiguous way to define a position $x_{sp} \neq a/2 + h$ such that $v(x_{sp}) = 0$. In other words, for a GL the notion of slip plane, or for that matter the concept of electrokinetic potential, loses any physical relevancy. This was already recognized for spherical polyelectrolytes,[11] but the conclusion holds for any soft structure. Interpretations of electrokinetic data for various soft materials in terms of ζ-potentials should necessarily integrate beforehand careful analysis of the hydrodynamic profiles so as to clearly define the positioning chosen for the virtual slip plane. In the following, the electrokinetic analysis will be performed introducing the only relevant potential difference for the system, that is, the Donnan potential.

4. Electrostatics: Determination of the Potential Distribution across the Diffuse Interface

The electric potential $\psi(x)$ across the diffuse interface is related to the distribution of the fixed charge density $\rho_{fix}(x)$, stemming from the spatial distribution of the charged polymer segments $\phi(x)$ across the interface (see section 2), and the charge density due to mobile electrolyte ions $\rho_{el}(x)$ by the Poisson equation

$$\frac{d^2\psi(x)}{dx^2} = -\frac{\rho_{fix}(x) + \rho_{el}(x)}{\epsilon_o\epsilon} \tag{31}$$

with ϵ_o and ϵ the dielectric permittivity of vacuum and the relative dielectric permittivity of water, respectively. In eq 31, it is tacitly assumed that the dielectric permittivity in the bulk gel and in the diffuse interface equals that of water. This is appropriate for highly hydrated layers, in accordance with the choice of the Stokes equation for the modeling of $k(x)$ (section 2). Within the Debye−Hückel (DH) approximation, the Boltzmann equation, which relates the ion concentrations inside and outside the GL to the potential distribution, is linearized so that for sufficiently moderate potentials $\psi(x)$, eq 31 reads

$$\frac{d^2y(x)}{dx^2} - \kappa^2 y(x) = -\frac{e}{k_B T\epsilon_o\epsilon}\rho_{fix}(x) \tag{32}$$

where we have introduced the reduced potential $y(x) \equiv e\psi(x)/k_BT$, with e the elementary charge, k_B the Boltzmann constant, and T the absolute temperature. The numerical analysis of eq 31 for diffuse charged layers with high Donnan potentials (nonlinearized Poisson−Boltzmann equation) and the implications for their electrokinetic response will be addressed separately.[40] κ is the reciprocal Debye length given by

$$\kappa = \left(\frac{2n_\infty e^2}{k_B T\epsilon_o\epsilon}\right)^{1/2} \tag{33}$$

with n_∞ the number of ions per unit volume in the bulk solution. The boundary conditions pertaining to eq 32 express continuity and the choice of a reference potential

$$y(x)|_{(a/2-\alpha)^-} = y(x)|_{(a/2-\alpha)^+}$$
$$\frac{dy(x)}{dx}|_{(a/2-\alpha)^-} = \frac{dy(x)}{dx}|_{(a/2-\alpha)^+} \tag{34a,b}$$

$$y(x)|_{(a/2+\alpha)^-} = y(x)|_{(a/2+\alpha)^+}$$
$$\frac{dy(x)}{dx}|_{(a/2+\alpha)^-} = \frac{dy(x)}{dx}|_{(a/2+\alpha)^+} \tag{35a,b}$$

$$\frac{dy(x)}{dx}|_{x\gg a/2+\alpha} = 0 \qquad y|_{x\gg a/2+\alpha} = y^D \tag{36a,b}$$

$$\frac{dy(x)}{dx}|_{x\to 0} = 0 \qquad y|_{x\to 0} = 0 \tag{37a,b}$$

where y^D is the Donnan potential. The solution satisfying eqs 32−37 is straightforward,

$$y(x) = \begin{cases} \dfrac{y^D}{2}\dfrac{\sinh(\kappa\alpha)}{\kappa\alpha}\exp[\kappa(x - a/2)] & \text{for } 0 \le x \le a/2 - \alpha \\ \dfrac{y^D}{2}\left\{1 + \dfrac{x - a/2}{\alpha} - \dfrac{\exp(-\kappa\alpha)}{\kappa\alpha}\sinh[\kappa(x - a/2)]\right\} & \text{for } a/2 - \alpha \le x \le a/2 + \alpha \\ y^D\left\{1 - \dfrac{1}{2}\dfrac{\sinh(\kappa\alpha)}{\kappa\alpha}\exp[-\kappa(x - a/2)]\right\} & \text{for } a/2 + \alpha \le x \le a/2 + h \end{cases} \tag{38a−c}$$

and y^D is derived from the local electroneutrality condition in the bulk gel, which yields

$$y^D = \frac{\rho_o}{2en_\infty} \tag{39}$$

Figure 3 illustrates the effect of α on the overall potential distribution across the diffuse interface. The symmetry of the patterns $y(x)$ with respect to the position $a/2$ (see expressions 38) is in accordance with the symmetry of the profile adopted for ρ_{fix} and the DH approximation. In this framework, the potential decay in the space charge layer equals that in the solution.[20] For $\alpha = 0$, the distribution of polymer segments in the GL is uniform and one easily verifies that $\phi(x)$ reduces to the expressions given by Ohshima in the limit of low $y^D - y(x)$,[20] that is, $y(x) = (y^D/2)\exp[\kappa(x - a/2)]$ and $y(x) = y^D\{1 - (1/2)\exp[-\kappa(x - a/2)]\}$ for $x \le a/2$ and $x \ge a/2$, respectively. The larger $\kappa\alpha$, the less steep the potential decay across the interface, in line with the slope

$$dy/dx|_{a/2} = (y^D/2\alpha)[1 - \exp(-\kappa\alpha)] \tag{40}$$

In a certain manner, the electrostatics for a GL is analogous to that of semiconductors, where the limited number of charge carriers gives rise to a spatial distribution of charge within the so-called space charge layer. The resulting charge density profile is related to the local concentrations of electrons and holes (and eventually of interstitials and vacancies) obtained from Boltzmann distributions involving the potential $y(x)$. First integration of the Poisson equation is then easily performed, leading to the electric field distribution in the semiconductor phase. Second integration to obtain the potential distribution requires numerical analysis. Following this strategy here, we may have written $\rho_{fix}(x)$ as a function of $\exp[y(x)]$. Nonetheless, there is a priori hardly any physical reason to do so and the hydrodynamics for such a spatial functionality (section 3) calls for more advanced mathematical tools, which necessarily complicate the problem without offering new fundamental physical insights.

(40) Duval, J. F. L. *Langmuir*, to be submitted.

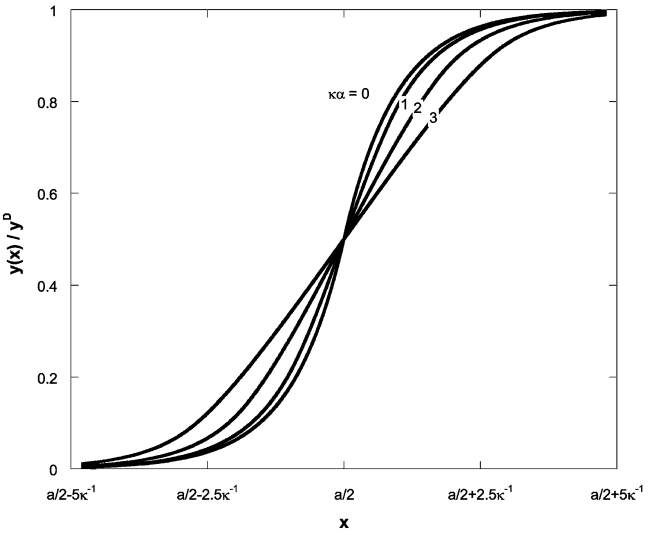

Figure 3. Spatial distribution of the electrostatic potential across the diffuse interface for various values of $\kappa\alpha$. $c_\infty = 1$ mM, $\rho_o = 1$ mM ($\psi^D = 12.8$ mV, $y^D \approx 0.5$).

5. Electrokinetics of Heterogeneous Charged Layers

5.1. Streaming Current. The streaming current I_{str} results from the lateral displacement of mobile ionic charges present inside *and* outside the GLs under the action of the applied pressure gradient $\Delta P/L_o$. For the geometry considered here, I_{str} is given by

$$I_{str} = 2l \int_0^{a/2+h} \rho_{el}(x) v(x)\, dx \tag{41}$$

where the factor 2 stems from the symmetry of the two-layer problem with respect to the position $x = 0$ (see Figure 1B). The solution given for the electrostatic problem implies nonoverlapping double layers. Within the framework of this assumption ($\kappa a \gg 1$), I_{str} is split into its three constituents

$$I_{str} = 2l\left(\int_0^{a/2-\alpha} \rho_{el}(x) v(x)\, dx + \int_{a/2-\alpha}^{a/2+\alpha} \rho_{el}(x) v(x)\, dx + \int_{a/2+\alpha}^{a/2+h} \rho_{el}(x) v(x)\, dx\right) \tag{42}$$

where the integrals refer to the currents streaming in the solution ($I_{str,sol}$), in the diffuse interface ($I_{str,diff\ int}$), and in the bulk GL ($I_{str,bulk\ GL}$). Within the DH approximation, $\rho_{el}(x)$ is simply written as

$$\rho_{el}(x) = 2n_\infty e y(x) \tag{43}$$

so that a positive streaming current I_{str} refers to the case $y^D > 0$ (arbitrary choice). Taking into account the relevant expressions derived in sections 3 and 4 for $v(x)$ and $y(x)$, respectively, one obtains for $I_{str,sol}$, $I_{str,diff\ int}$, and $I_{str,bulk\ GL}$ in the limit $\kappa a \gg 1$

$$I_{str,sol} = \frac{y^D e l n_\infty}{\kappa}\left(2v_0 + \frac{\Delta P a}{\eta_w L_o \kappa}\right)\left(\frac{1 - \exp(-2\kappa\alpha)}{2\kappa\alpha}\right) \tag{44}$$

$$I_{str,diff\ int} = 2y^D e l n_\infty \alpha\left[\sum_{n=0}^{\infty} \frac{2^{n+2} v_n}{n+2} - \frac{\exp(-\kappa\alpha)}{\kappa\alpha} \sum_{n=0}^{\infty} v_n \int_0^2 u^n \sinh[\kappa\alpha(u-1)]\, du\right] \tag{45}$$

$$I_{str,bulk\ GL} = 4y^D e l n_\infty \left\{\frac{\Delta P}{\eta_w L_o \lambda_o^2}(h - \alpha) + [1 - \exp(\lambda_o(\alpha - h))]\left(\frac{C_3 + C_4}{\lambda_o}\right) + \frac{\sinh(\kappa\alpha)}{2\kappa\alpha} \times \exp(-\kappa h)\left[\frac{\Delta P}{\eta_w L_o \lambda_o^2 \kappa}[1 - \exp(\kappa(h - \alpha))] + \frac{C_3}{\kappa + \lambda_o}(\exp[\lambda_o(\alpha - h)] - \exp(\kappa(h - \alpha))) + \frac{C_4}{\kappa - \lambda_o}(1 - \exp(\kappa(h - \alpha) + \lambda_o(\alpha - h)))\right]\right\} \tag{46}$$

For $\alpha = 0$ and $\lambda_o^{-1} \to 0$, I_{str} reduces to

$$I_{str} = I_{str,sol} = \frac{y^D e l n_\infty \Delta P a}{L_o \eta_w \kappa^2} \tag{47}$$

which represents the Helmholtz−Smoluchowski equation for rigid surfaces,[41,42] with the potential y^D representing in that case twice the dimensionless electrokinetic potential. The limit $\alpha = 0$ corresponds to a uniform segment distribution in the GL, as assumed in the formalism reported by Ohshima.[9] This limit is written

$$I_{str_{\alpha=0}} = y^D e l n_\infty \frac{\Delta P}{\eta_w L_o}\left\{\frac{a}{\kappa^2} + \frac{2}{\lambda_o^2 \kappa}\left[1 - \exp(-\lambda_o h) + \tanh(\lambda_o h)\left(\frac{a\lambda_o}{2} - \exp(-\lambda_o h)\right)\right] + 4\left\{\frac{h}{\lambda_o^2} + \frac{1 - \exp(-\lambda_o h)}{\lambda_o^3}\left[\frac{(\exp(\lambda_o h) - 1)}{2\cosh(\lambda_o h)}\left(\frac{a\lambda_o}{2} - \exp(-\lambda_o h)\right) - 1\right]\right\} + \frac{2}{\lambda_o^2 \kappa}[\exp(-\kappa h) - 1]\right\} + 2y^D e l n_\infty \left\{\frac{C_3}{\kappa + \lambda_o}[\exp(-h(\lambda_o + \kappa)) - 1] + \frac{C_4}{\kappa - \lambda_o}[\exp(-\kappa h) - \exp(-\lambda_o h)]\right\} \tag{48a}$$

with

$$C_3 = \frac{1}{1 + \exp(-2\lambda_o h)} \frac{\Delta P}{\eta_w L_o \lambda_o^2}\left(\frac{a\lambda_o}{2} - \exp(-\lambda_o h)\right) \tag{48b}$$

and

$$C_4 = -\frac{\Delta P}{\eta_w L_o \lambda_o^2}\left[1 + \frac{1}{2\cosh(\lambda_o h)}\left(\frac{a\lambda_o}{2} - \exp(-\lambda_o h)\right)\right] \tag{48c}$$

In Figure 4, the normalized streaming current $I_{str}/I_{str_{\alpha=0}}$ is plotted versus $\kappa\alpha$ for various $\kappa\lambda_o^{-1}$ at given n_∞ and ρ_o (constant y^D). In Figure 4b, the corresponding values $I_{str_{\alpha=0}}$ (normalized by the pressure ΔP) are given for purposes of comparison. The results refer to the situations of practical interest where $h \gg \alpha$ and $\kappa h \gg 1$. The more penetrable the GL for ions from the solution, the less

(41) Von Helmholtz, H. *Ann. Phys.* **1879**, *7*, 337.
(42) Von Smoluchowski, M. *Bull. Int. Acad. Sci. Cracovie* **1903**, 184. Von Smoluchowski, M. *Handbuch der Electrizität und des Magnismus*; Graetz, W., Ed.; Barth: Leipzig, 1914; Vol. II, p 366. Von Smoluchowski, M. *Z. Phys. Chem.* **1918**, *92*, 129.

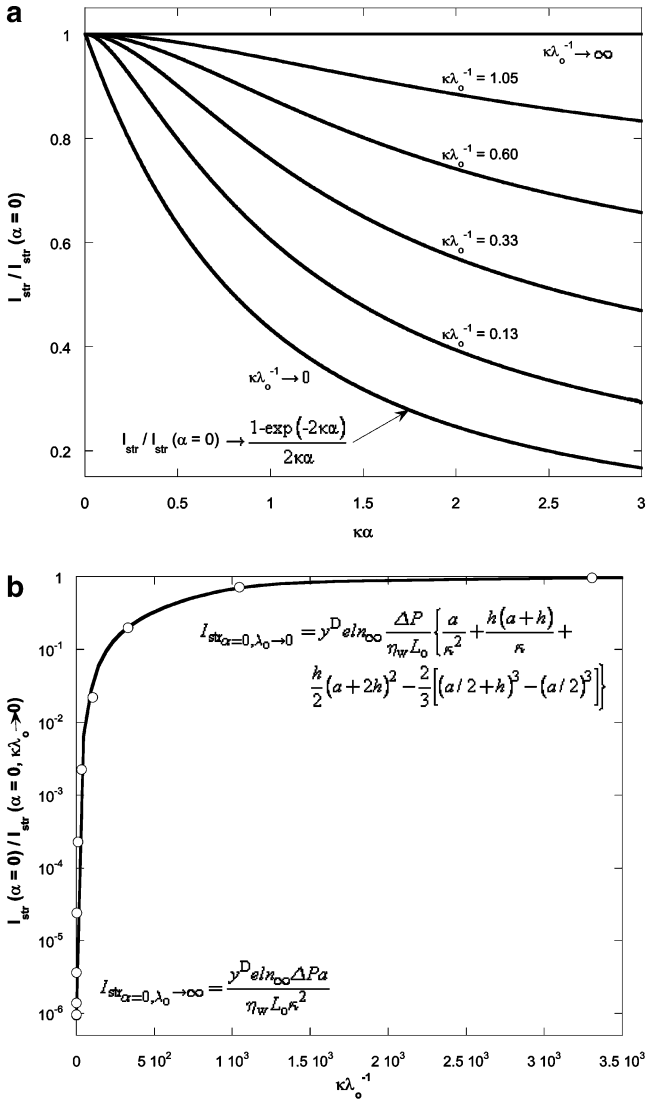

Figure 4. (a) Streaming current as a function of $\kappa\alpha$ for different hydrodynamic penetration lengths λ_o^{-1} (indicated). $c_\infty = 1$ mM, $\psi^D = 12.8$ mV, and $\kappa h = 10^3$. The results are normalized with respect to $I_{str_{\alpha=0}}$, current which corresponds to a uniform distribution of the polymer segments in the charged layer (Ohshima's formalism). In panel b, $I_{str_{\alpha=0}}$ is set against $\kappa\lambda_o^{-1}$ and the analytical expressions in the limits $\kappa\lambda_o^{-1} \to 0$ and $\kappa\lambda_o^{-1} \to \infty$ are given for $\kappa h \gg 1$.

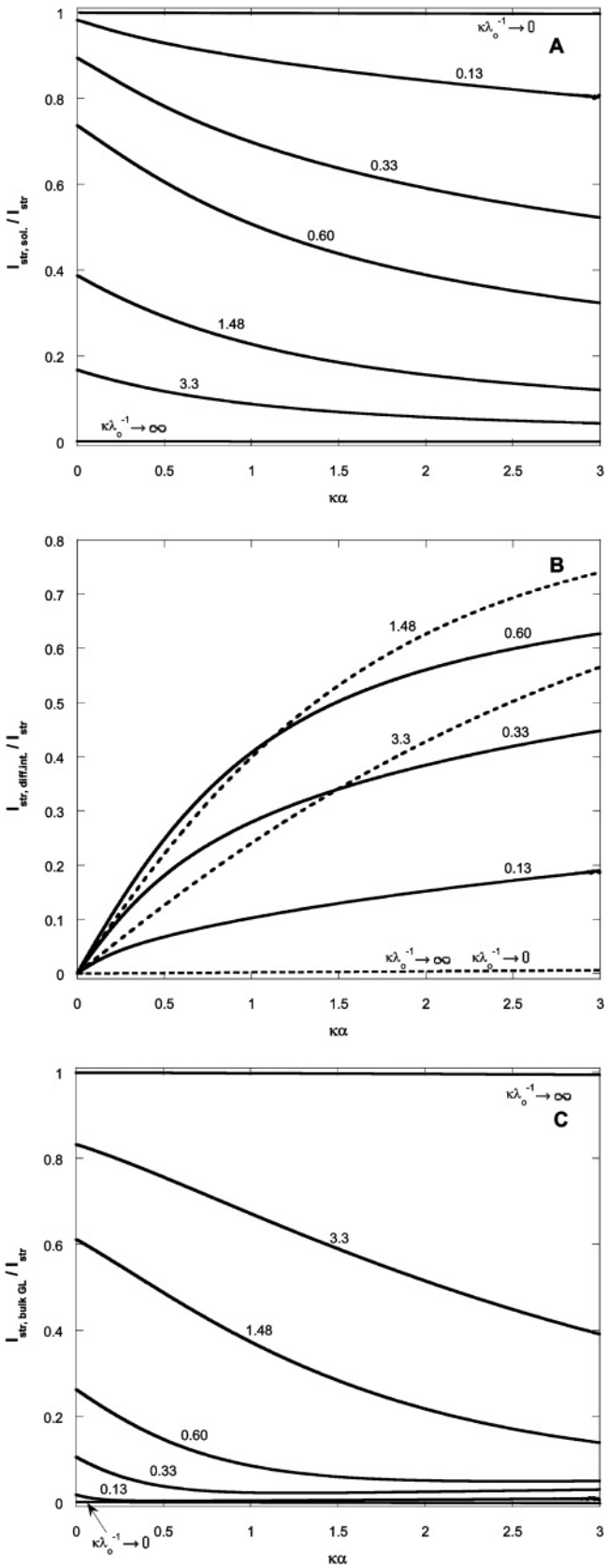

Figure 5. Respective contributions of (panel A) $I_{str,sol}$, (panel B) $I_{str,diff\ int}$, and (panel C) $I_{str,bulk\ GL}$ to the total current I_{str} streaming in the thin-layer chamber (which includes the charged layers). The parameters are the same as in Figure 4.

pronounced the influence of α on the electrokinetic response. The component $I_{str,bulk\ GL}$ increases (Figure 5C), and in the limit $\kappa\lambda_o^{-1} \to \infty$ it predominantly determines I_{str}. The lateral flux of counterions in the bulk GL largely exceeds those in the diffuse interface and in the solution ($h \gg \alpha, y^D > y(x)$) and thus constitutes a major contribution to I_{str}. For lower $\kappa\lambda_o^{-1}$ (a more rigid GL), the flow velocity inside the bulk GL decreases (Figure 2A), which reduces $I_{str,bulk\ GL}/I_{str}$ (Figure 5C) and clarifies the effect of α on I_{str}. At a given $\kappa\lambda_o^{-1}$, I_{str} decreases with increasing $\kappa\alpha$. On the basis of Figure 3 only, this result might seem surprising. Indeed, an increase in $\kappa\alpha$ actually corresponds to an increase of the potential $y(x)$ and the local electrolyte concentration in the region $x < a/2$, where the fluid velocity v is the most significant (Figure 2B). However, extending the thickness of the diffuse interface also results in a decrease of v (and of $v(x = 0)$) in the region where there is an excess of electrokinetically active counterions ($a/2 - \alpha < x < a/2$). This hydrodynamic effect overrules the electrostatic effect and is responsible for the decrease of the total current I_{str} upon increasing α.

Let us now have a closer look at the dependencies of the three contributions to I_{str} on α and $\kappa\lambda_o^{-1}$. The fraction $I_{str,sol}/I_{str}$ (Figure 5A) decreases with increasing $\kappa\lambda_o^{-1}$ and/or α for reasons already mentioned (increase of $I_{str,bulk\ GL}/I_{str}$ and decrease of v, respectively). Panels B and C of Figure 5 represent $I_{str,diff\ int}/I_{str}$ and $I_{str,bulk\ GL}/I_{str}$, respectively. For a given α, the influence of $\kappa\lambda_o^{-1}$ on $I_{str,bulk\ GL}/I_{str}$ has already been discussed. Increasing α at low $\kappa\lambda_o^{-1}$ reduces the local electrolyte concentration in the part of the bulk GL which is hydrodynamically active (Figure 3), thus resulting in a decrease of $I_{str,bulk\ GL}/I_{str}$. Upon further increase of α, $I_{str,bulk\ GL}/I_{str}$ passes through a shallow minimum. The presence of this minimum is caused by a significant increase of v at the edge of the bulk GL as resulting from the decrease of the local friction coefficients in the region $a/2 < x < a/2 + \alpha$ with increasing α (hydrodynamic effect). For higher $\kappa\lambda_o^{-1}$, the minimum is displaced toward larger values of α and the effect of α gradually vanishes (the bulk GL with thickness $h \gg \alpha$ becomes entirely hydrodynamically active). At given $\kappa\lambda_o^{-1}$, the fraction $I_{str,diff\ int}/I_{str}$ increases for the whole range of α considered because of the increasing number of counterions in the diffuse interface. One can distinguish two regimes: for small α, the increase in $I_{str,diff\ int}/I_{str}$ is steep, and the hydrodynamics does not limit the fraction of mobile counterions. For higher α, the hydrodynamics plays a limiting role in the electrokinetics of the diffuse interface (decrease of v) and the curves start to bend. In the limits $\kappa\lambda_o^{-1} \to 0$ and $\kappa\lambda_o^{-1} \to \infty$, only a small fraction of the total current flows in the diffuse interface because it is inaccessible for ions and the contribution of the current in the bulk GL is dominant, respectively.

The effects of the fixed charge density ρ_o and the thickness h of the layer on the electrokinetics are straightforward. Within the DH approximation, the current I_{str} is proportional to the Donnan potential y^D and therefore to ρ_o (see eqs 44−46). The curves $I_{str}/I_{str_{\alpha=0}}$ in Figure 4 remain unchanged. With increasing h at fixed α and $\kappa\lambda_o^{-1}$, I_{str} increases due to the increase of $I_{str,bulk\ GL}$. Roughly speaking, the effect is similar to that of $\kappa\lambda_o^{-1}$ as discussed earlier. For $\kappa\lambda_o^{-1} \to 0$, the electrokinetics becomes independent of h, as expected.

More interesting is the analysis of the electrokinetic response of the GLs for different electrolyte concentrations n_∞ at various α and fixed hydrodynamic penetration depth λ_o^{-1} (Figure 6). At high n_∞ ($\kappa^{-1} \to 0$), the streaming current reaches a finite limiting value. This peculiar feature characterizes soft interfaces and differentiates them from hard interfaces for which the electrokinetic response in concentrated electrolytes vanishes. Analogously, the electrophoretic mobility of a soft spherical particle asymptotically tends to a constant value for $n_\infty \to \infty$.[9] An expression for $I_{str_{\kappa^{-1}\to 0}}$ can be derived from eqs 44−46:

$$I_{str_{\kappa^{-1}\to 0}} \approx 4y^D el n_\infty \left\{ \alpha \sum_{n=0}^{\infty} \frac{2^{n+1} v_n}{n+2} + \frac{\Delta P}{\eta_w L_o \lambda_o^2}(h - \alpha) + \frac{C_3 + C_4}{\lambda_o}[1 - \exp(-\lambda_o(\alpha - h))] \right\} \quad (49)$$

The terms in eq 49 stem from the current flowing in the diffuse interface and bulk gel layer. The latter overrules the former for $h \gg \alpha$, as valid for the computations presented in Figure 6. With decreasing n_∞ (increasing y^D), the streaming current increases for any α: this is a generic feature for electrokinetics of ionic double layers. With increasing $\kappa\alpha$, the overall streaming current I_{str} decreases as demonstrated in Figure 4. The new element is that this decrease is more pronounced the lower n_∞. For $c_\infty = n_\infty/N_a = 0.2$ mM ($\kappa^{-1} = 19$ nm, N_a is the Avogadro number) and $\kappa\alpha = 2.6$, the streaming current value is about 40% of that for $\kappa\alpha = 0$. In the low concentration range, the ionic charges are distributed over large distances and the increase of the local friction coefficients within the spatial range [0, $a/2$] effectively immobilizes a large fraction of counterions. In many studies on the electrokinetics of soft surfaces, the theory by Ohshima based on a uniform segment distribution largely overestimates experimental results obtained at low electrolyte concentrations.[26−29] Figure 6 illustrates (one of) the reason(s) for this discrepancy between theory and experiment: the lower the n_∞, the more critical the structural details of the GL for the electrokinetics.

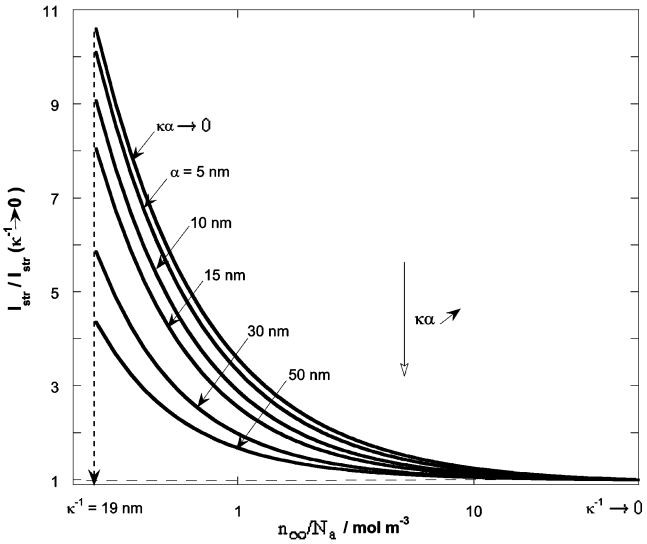

Figure 6. Representation of I_{str} as a function of the electrolyte concentration c_∞ for various thicknesses α (indicated) of the diffuse interface. The results are normalized with respect to $I_{str_{\kappa^{-1}\to 0}}$, reached for $c_\infty \gg 1$. $\rho_o = 0.5$ mM, $h = a/2$, $\lambda_o^{-1} = 3.2$ nm.

5.2. Back-Conduction Currents. Provided the resistance of the external circuit used to perform the electrokinetic measurements is very high, a potential difference $\Delta\varphi_{str}$ builds up across the capillary (Figure 1B) as a result of the flow of counterions. The resulting electric field leads to a countercurrent, denoted I_b. In the steady-state, the following relation applies:

$$I_{str} = I_b \quad (50)$$

Two contributions for I_b may be distinguished: the current originating from the migration of the counterions under the action of the electric field $E = \Delta\varphi_{str}/L_o$, denoted I_{mig}, and the current produced by the electroosmotic flow resulting from the action of the field on the diffuse double layer, denoted I_{eo}.

5.2.1. Expression for I_{mig}. Within the DH approximation, the migration component of the total countercurrent for a 1:1 electrolyte is simply given by

$$I_{mig} = 2lEc_\infty \int_0^{a/2+h} \{\lambda_+(x) + \lambda_-(x) + y(x)[\lambda_-(x) - \lambda_+(x)]\}\, dx \quad (51)$$

with $\lambda_\pm$ the molar conductivities of the cations and anions. Because of the steric, electrostatic, and specific interactions between ions and polymer segments inhomogeneously distributed in the GLs, molar conductivities are expected

to be a function of the position x. As mentioned earlier, the layers commonly encountered in practice are highly hydrated so that the transport characteristics of ions inside and outside the porous structure are very similar, as demonstrated by various experimental studies on the diffusion coefficients of ions in hydrogels.[43] Therefore, in the following we shall consider $\lambda_\pm$ to be constant and equal to the bulk aqueous solution values. For concentrated gels with water contents far below 100%, this simplification has to be revisited. Noting that $\lambda_{salt} = \lambda_+ + \lambda_-$ and introducing the dimensionless parameter $\Delta\lambda$,

$$\Delta\lambda = \frac{\lambda_- - \lambda_+}{\lambda_- + \lambda_+} \tag{52}$$

one obtains after straightforward rearrangement

$$I_{mig} = 2lEc_\infty\lambda_{salt}\left[\frac{a}{2} + h(1 + \Delta\lambda y^D) + \kappa^{-1}\frac{\Delta\lambda y^D}{2}\frac{\sinh(\kappa\alpha)}{\kappa\alpha}\exp(-\kappa h)\right] \tag{53}$$

which is valid for $\kappa a \gg 1$. The second term within brackets in eq 53 stems from the ionic conduction in the GL. Under most experimental conditions, that term is responsible for significant deviation of the streaming potential compared to its Helmholtz−Smoluchowski value for rigid surfaces.

5.2.2. Expression for I_{osm}. To obtain the convective contribution to I_b, the electroosmotic flow profile $v_{eo}(x)$ is required. The latter derives from the Navier−Stokes equation for stationary flow in the incompressible limit

$$\frac{d^2v_{eo}(x)}{dx^2} - \frac{k(x)}{\eta_w}v_{eo}(x) = -\Gamma E y(x) \tag{54}$$

with $k(x)$ as defined in section 2 and $\Gamma = 2en_\infty/\eta_w$. The boundary conditions pertaining to eq 54 remain as given by eqs 7−10 after replacing $v(x)$ by $v_{eo}(x)$. As for eqs 4−6, hydrodynamic interactions are not taken into account so that friction forces remain proportional to velocities. For reasons of symmetry, the analysis is only performed for $x > 0$. General solutions of eq 54 for the regions corresponding to the electrolyte solution and the bulk GL are

$0 \le x \le a/2 - \alpha$:

$$v_{eo}(x) = -\Gamma E\left\{\frac{y^D}{2\kappa^2}\frac{\sinh(\kappa\alpha)}{\kappa\alpha}\exp[\kappa(x - a/2)]\right\} + D_1x + D_2 \tag{55}$$

$a/2 + \alpha \le x \le a/2 + h$:

$$v_{eo}(x) = \Gamma E y^D\left(\frac{1}{\lambda_o^{-2}} + \frac{1}{\kappa^2 - \lambda_o^{-2}}\frac{\sinh(\kappa\alpha)}{2\kappa\alpha}\exp[-\kappa(x - a/2)]\right) + D_3\exp\left[\frac{-x + (a/2 + \alpha)}{\lambda_o^{-1}}\right] + D_4\exp\left[\frac{x - (a/2 + h)}{\lambda_o^{-1}}\right] \tag{56}$$

where $(D_i)_{0\le i\le 4}$ are constants. To obtain the solution $v_{eo}(x)$ in the diffuse interface, we first write the Taylor expansion of the corresponding potential (eq 38b) in the vicinity of $x = a/2$:

$$y(x) = \frac{y^D}{2}\left\{u(x) - \sum_{k=0}^{\infty}\frac{(\kappa\alpha)^{2k}\exp(-\kappa\alpha)}{(2k+1)!}(u(x) - 1)^{2k+1}\right\} \tag{57}$$

Using the binomial formula to develop the product $(u(x) - 1)^{2k+1}$ in eq 57 and changing variables, eq 54 for $a/2 - \alpha < x < a/2 + \alpha$ may be written in the form

$$\frac{d^2v_{eo}(x)}{du^2} - \theta u v_{eo}(x) = -\Gamma E\alpha^2\sum_{k=0}^{\infty}\tilde{y}_k u^k \tag{58}$$

where the coefficients $\tilde{y}_k$ in the polynome in $u(x)$ describe the distribution $y(x)$ in the diffuse interface. Adopting the strategy followed to obtain $v(x)$ in the diffuse interface (eq 12), we obtain the series expansion for $v_{eo}(x)$

$a/2 - \alpha \le x \le a/2 + \alpha$:

$$v_{eo}(x) = v_{eo_0} + v_{eo_1}u(x) + v_{eo_2}[u(x)]^2 + \sum_{j=0}^{2}\sum_{n=1}^{\infty}v_{eo_{3n+j}}[u(x)]^{3n+j} \tag{59}$$

with

$$v_{eo_2} = -\frac{\Gamma E\alpha^2}{2}\tilde{y}_0 \tag{60}$$

and

$$(v_{eo_{3n+j}})_{n\ge 1, 0\le j\le 2} = \theta^n\frac{j!}{(3n+j)!}f(n,j)v_{eo_j} - \frac{\Gamma E\alpha^2}{(3n+j)!}\sum_{k=1}^{n}\tilde{y}_{3n-(3k-j-1)}[3n - (3k - j - 1)]!\theta^{k-1}g(n,k,j) \tag{61}$$

where g is the function defined by

$$g(n,k,j) = \begin{cases}\prod_{p=n-k+1}^{n-1}(3p + j + 1) \text{ if } k \ne 1\\ 1, \text{ otherwise}\end{cases} \tag{62}$$

To completely solve the profile $v_{eo}(x)$ for any x, we require the constants $(D_i)_{0\le i\le 4}$ and $(v_{eo_i})_{i=0,1}$ yielded by the boundary

(43) Zhang, H.; Davison, W. *Anal. Chim. Acta* **1999**, *398*, 329.

conditions given by eqs 7−10 after replacing $v(x)$ by $v_{eo}(x)$. The result is that $D_1 = 0$ and

$$D_2 = v_{eo_0} + \Gamma E\left[\frac{y^D}{2\kappa^2}\frac{\sinh(\kappa\alpha)}{\kappa\alpha}\exp(-\kappa\alpha)\right] \quad (63)$$

$$v_{eo_1} = -\Gamma E\alpha\frac{y^D}{2\kappa}\frac{\sinh(\kappa\alpha)}{\kappa\alpha}\exp(-\kappa\alpha) \quad (64)$$

$$\Gamma E y^D\left(\frac{1}{\lambda_o^2} + \frac{1}{\kappa^2 - \lambda_o^2}\frac{1 - \exp(-2\kappa\alpha)}{4\kappa\alpha}\right) + D_3 + D_4\exp[\lambda_o(\alpha - h)] - \sum_{j=0}^{2}\left\{2^j v_{eo_j}\left(1 + \sum_{n=1}^{\infty}\theta^n\frac{2^{3n}j!}{(3n+j)!}f(n,j)\right) - \Gamma E\alpha^2\sum_{n=1}^{\infty}\sum_{k=1}^{n}\frac{2^{3n+j}}{(3n+j)!}\tilde{y}_{3n-(3k-j-1)}[3n - (3k - j - 1)]!\theta^{k-1}g(n,k,j)\right\} = 0 \quad (65)$$

$$-\Gamma E y^D\left[\frac{1 - \exp(-2\kappa\alpha)}{4(\kappa^2 - \lambda_o^2)}\right] + (2\theta)^{1/2}(D_4\exp[\lambda_o(\alpha - h)] - D_3) - \sum_{j=0}^{2}\left\{v_{eo_j}\left(j^2 + \sum_{n=1}^{\infty}\theta^n\frac{2^{3n+j-1}j!}{(3n+j-1)!}f(n,j)\right) - \Gamma E\alpha^2\sum_{n=1}^{\infty}\sum_{k=1}^{n}\frac{2^{3n+j-1}}{(3n+j-1)!}\tilde{y}_{3n-(3k-j-1)}[3n - (3k - j - 1)]!\theta^{k-1}g(n,k,j)\right\} = 0 \quad (66)$$

$$D_4 = -\Gamma E y^D\left(\frac{1}{\lambda_o^2} + \frac{1}{\kappa^2 - \lambda_o^2}\frac{\sinh(\kappa\alpha)}{2\kappa\alpha}\exp(-\kappa h)\right) - D_3\exp[\lambda_o(\alpha - h)] \quad (67)$$

Solving the system of linear eqs 63−67 in $(D_i)_{0\le i\le 4}$ and $(v_{eo_i})_{i=0,1}$ is straightforward. The electroosmotic current I_{eo} is then obtained from

$$I_{eo} = 2l\int_0^{a/2+h}\rho_{el}(x)v_{eo}(x)\,dx \quad (68)$$

and analytical expressions for the three constituents $I_{eo,sol}$, $I_{eo,diff\ int}$, and $I_{eo,bulk\ GL}$ may be given as

$$I_{eo,sol} = \frac{2eln_\infty}{\kappa}\left[\frac{-\Gamma E}{4\kappa^2}\left(\frac{y^D\sinh(\kappa\alpha)}{\kappa\alpha}\right)^2\exp(-2\kappa\alpha) + \frac{1 - \exp(-2\kappa\alpha)}{2\kappa\alpha}D_2 y^D\right] \quad (69)$$

$$I_{eo,diff\ int} = 2y^D eln_\infty\alpha\left[\sum_{n=0}^{\infty}\frac{2^{n+2}v_{eo_n}}{n+2} - \frac{\exp(-\kappa\alpha)}{\kappa\alpha}\sum_{n=0}^{\infty}v_{eo_n}\int_0^2 u^n\sinh[\kappa\alpha(u-1)]\,du\right] \quad (70)$$

$$I_{eo,bulk\ GL} = 4y^D eln_\infty\left\{\frac{\Gamma E y^D}{\lambda_o^2}(h - \alpha) + [1 - \exp(\lambda_o(\alpha - h))]\left(\frac{D_3 + D_4}{\lambda_o}\right) + \frac{\sinh(\kappa\alpha)}{2\kappa\alpha}\exp(-\kappa h)\left\{\Gamma E y^D\left[(1 - \exp[\kappa(h - \alpha)])\left(\frac{1}{\kappa\lambda_o^2} + \frac{1}{\kappa(\lambda_o^2 - \kappa^2)}\right) + \frac{1}{2\kappa(\kappa^2 - \lambda_o^2)}\frac{\sinh(\kappa\alpha)}{2\kappa\alpha}\{\exp(-\kappa h) - \exp[\kappa(h - 2\alpha)]\}\right] + \frac{D_3}{\kappa + \lambda_o}(\exp[\lambda_o(\alpha - h)] - \exp[\kappa(h - \alpha)]) + \frac{D_4}{\kappa - \lambda_o}\{1 - \exp[\kappa(h - \alpha) + \lambda_o(\alpha - h)]\}\right\}\right\} \quad (71)$$

5.2.3. Results and Discussion. In Figure 7, the normalized velocity of the electroosmotic flow, $v_{eo}(x)/v_{eo}(x = 0)$, is represented for various values of $\kappa\lambda_o^{-1}$ and $\kappa\alpha$. The values of $v_{eo}(x = 0)$ as a function of $\kappa\lambda_o^{-1}$ are also reported in the inset for quantitative comparison of the data. With increasing hydrodynamic penetration length λ_o^{-1}, $v_{eo}(x)$ increases for every x (panel A), as expected. In the bulk solution outside the double layer region ($x \ll a/2 - \kappa^{-1}$), the local concentration of ions approaches n_∞, the local electric field is zero, and $v_{eo}(x) \to v_{eo}(0)$. In the bulk of the GL, $y(x) = y^D$, $\lambda^{-1}(x) = \lambda_o^{-1}$ and $v_{eo}(x)$ barely depends on position while dropping to zero at the edge of the GL in accordance with the imposed condition $v_{eo}(a/2 + h) = 0$. For positions x corresponding to significant variations of the local potential $y(x)$, $v_{eo}(x)$ exhibits a minimum. The presence of that minimum is explained by the difference between the characteristic lengths describing the potential and the friction coefficient distributions, viz., κ^{-1} and α, respectively (see Figure 3). For given α and λ_o^{-1} (panel A), starting from a position $x = x_o$ in the bulk GL, $y(x)$ decreases with decreasing x whereas k remains equals to its bulk GL value. Consequently, the local electrolyte concentration decreases and so does $v_{eo}(x)$. Upon further decrease of x, decrease of the friction coefficient compounds the decrease of the local electrolyte concentration. As a result, $v_{eo}(x)$ increases. In agreement with the explanation given above, the minimum is located around $x = a/2 + \alpha$ and gradually disappears when increasing $\kappa\lambda_o^{-1}$. The dependence of $v_{eo}(x)$ on α at constant λ_o^{-1} is illustrated in panel B of Figure 7. Upon increase of $\kappa\alpha$, the width of the minimum of $v_{eo}(x)$ increases and $v_{eo}(0)$ decreases (not shown), which is consistent with the broader spatial transition for $k(x)$. At given x, the relative electroosmotic velocity increases (decreases) for $x > a/2$ ($x < a/2$), as a result of the decrease (increase) of the corresponding local friction coefficients.

In Figure 8, the ratio I_{eo}/I_{mig} is plotted against the electrolyte concentration n_∞ for various values of λ_o^{-1}. For a given n_∞, the electroosmotic contribution to the total backcurrent increases steeply upon increase of λ_o^{-1} before asymptotically reaching a constant value in the limit $\kappa\lambda_o^{-1} \to \infty$. At a given λ_o^{-1}, the ratio I_{eo}/I_{mig} (which remains small in the condition of low Donnan potentials considered) increases with decreasing n_∞, as a result of the increase of I_{eo}. This is analogous to the increase of the surface conduction contribution (expressed by the Dukhin number Du[44]) in the electrokinetics of rigid surfaces with decreasing electrolyte concentration. For $h \gg \alpha$ (and thus $\kappa h \gg 1$), the currents I_{eo} and I_{mig} remain practically independent of the parameter α for low to moderate $\kappa\alpha$. Within these

(44) Dukhin, S. S. *Adv. Colloid Interface Sci.* **1993**, *44*, 1.

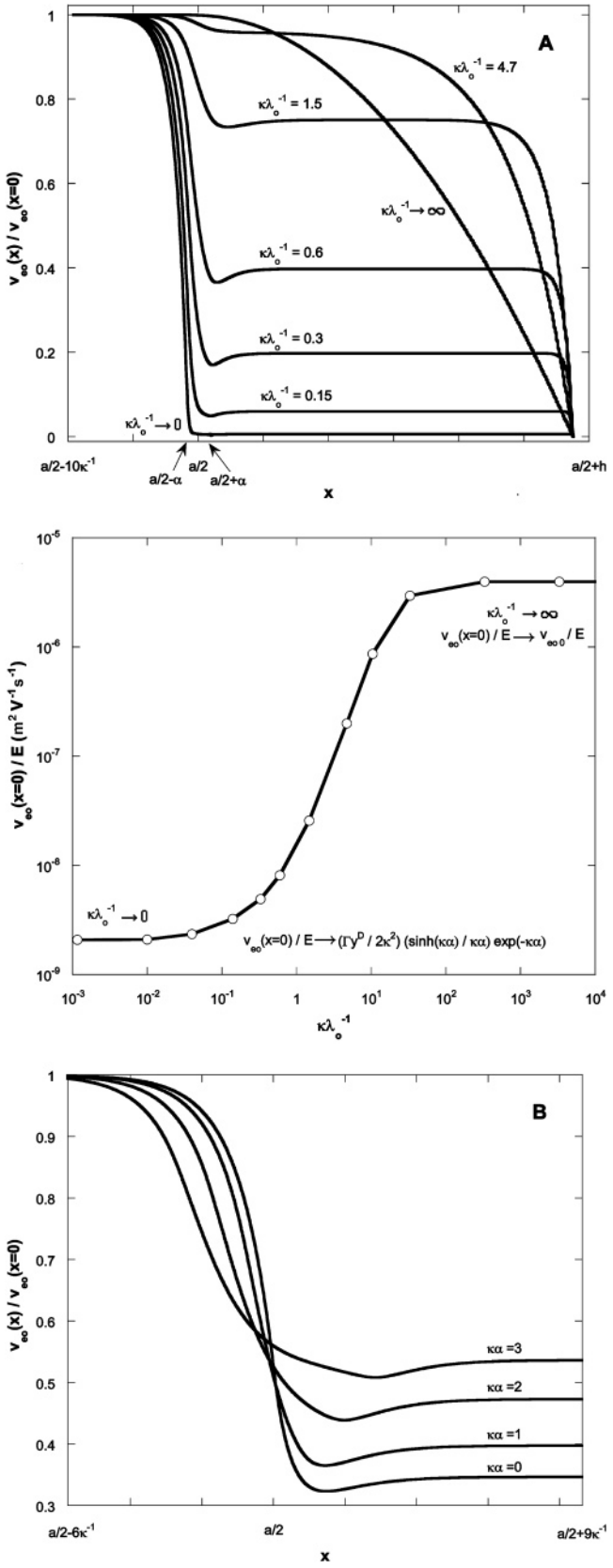

Figure 7. (Panel A) Spatial distribution of the (normalized) electroosmotic flow profile as a function of the softness of the charged layer. Below, the corresponding $v_{eo}(x = 0)$ (maximum electroosmotic velocity) is given. $c_\infty = 1$ mM, $\psi^D = 12.8$ mV ($\rho_o = 1$ mM), $\kappa h = 30$, $\kappa\alpha = 1$. (Panel B) Spatial distribution of the (normalized) electroosmotic flow profile as a function of $\kappa\alpha$. $\kappa\lambda_o^{-1} = 0.6$; other parameters are as in panel A.

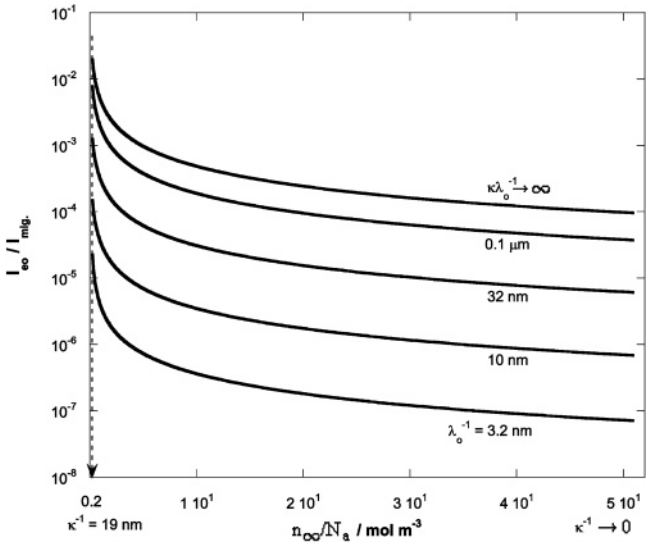

Figure 8. Ratio I_{eo}/I_{mig} as a function of the electrolyte concentration and λ_o^{-1} (indicated). $\rho_o = 0.5$ mM, $h/a = 10^{-3}$, $\alpha = 1$ nm. The parameters $\lambda_\pm$ required for the computation of I_{mig} refer to the ions Na^+ and Cl^-.

limits, for $\lambda_o h \gg 1$, I_{eo}/I_{mig} reduces to

$$I_{eo}/I_{mig} \approx \frac{2(y^D)^2 F\Gamma h}{\lambda_o^2 \lambda_{salt}\left(\frac{a}{2} + h(1 + \Delta\lambda y^D)\right)} \tag{72}$$

with F the Faraday constant.

5.3. Streaming Potential. Using eq 50, the streaming potential may be written in the form

$$\Delta\varphi_{str} = \frac{I_{str} L_o}{\mathscr{P}(K_{mig} + K_{eo})} \tag{73}$$

where $\mathscr{P}$ is the cross section $(a + 2h)l$ of the cell, K_{mig} ($=I_{mig}/\mathscr{P}E$) and K_{eo} ($=I_{eo}/\mathscr{P}E$) representing the conductivity terms originating from the conductive and electroosmotic components of the total back-current. Some authors prefer to express the overall back-current in terms of a bulk solution conduction current and *a surface conduction current* with two contributions, that is, the migration and electroosmotic currents within the GL. This leads to the introduction of a surface conductivity term in the expression of the streaming potential.[16] From a mathematical point of view, it is always possible to define such a term. Nevertheless there is a priori hardly a physical reason to do so since the physical statuses of the overall back-currents in the bulk solution and GLs of finite thickness are not fundamentally different. This motivates our preference for writing $\Delta\varphi_{str}$ in the form given by eq 73. Figure 9 illustrates the dependence of $\Delta\varphi_{str}/\Delta P$ on the electrolyte concentration and the parameter α within the conditions of Figure 6. As for I_{str}, $\Delta\varphi_{str}/\Delta P$ decreases with increasing $\kappa\alpha$ as a result of the decrease of the hydrodynamic velocity. The dependencies of $\Delta\varphi_{str}/\Delta P$ on h and λ_o^{-1} are similar to those for I_{str} (not shown). In the low electrolyte concentration regime, the electrokinetics is substantially affected by the inhomogeneity of the distribution of polymer segments in the GL. This leads to significant deviations from the results expected on the basis of Ohshima's theory ($\kappa\alpha = 0$), as observed in various experimental studies.[26−29] In a future communication,[28] streaming potential data collected for crossed-linked polyacrylamide gels with various ρ_o values in the range of 0.5−0.05 mM electrolyte concentration will be analyzed

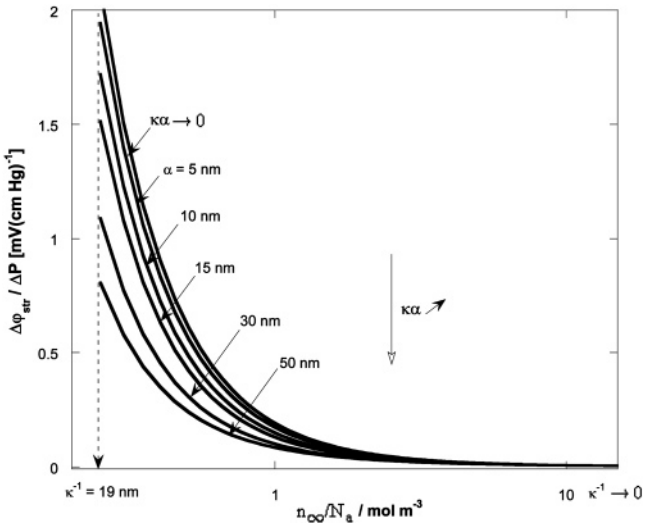

Figure 9. Streaming potential as a function of the electrolyte concentration and α (indicated). The parameters are the same as in Figure 6.

and discussed within the formalism presented in the current paper. It will be shown that (i) for low salt concentrations and/or high ρ_o, the assumption $\kappa\alpha = 0$ is very poor, if not totally inadequate, and (ii) structural changes of the diffuse interface with changing electrolyte concentration (swelling) are very well reproduced when analyzing experimental data with the concept of a diffuse interface, as introduced here.

6. Conclusions

A quantitative model is proposed for the electrokinetics of the gel/solution interfaces (the analysis is of general validity for other types of soft interfaces) characterized by ion permeability and a gradual transition from one phase to the other. Linear gradients for the gel density ϕ and charge density ρ are considered in the so-called *diffuse interface*, between bulk electrolyte solution and bulk gel layer. The analysis focuses on charged layers with high water contents for which the spatial distribution of the friction coefficient in the porous layer/electrolyte solution interphase follows that of ϕ and ρ, in accordance with Stokes' relationship. Analytical solutions are given for the electrostatic, hydrodynamic, and electroosmotic responses within the Debye−Hückel approximation. Subsequent derivations for the streaming current, the migration current, the electroosmotic current, and the streaming potential are given. The analysis clearly shows that the (coupled) electrostatic and hydrodynamic gradual transitions at the diffuse interface considerably affect the streaming potential/streaming current obtained when assuming a discontinuous segment distribution across the gel/solution interface. More exactly, the electrokinetic response of the latter decreases with increasing ratio between the thickness α of the diffuse interface and the Debye length κ^{-1}. The linear profiles for ϕ and ρ assumed in the current study are valid for low to moderate $\kappa\alpha$. The lower the electrolyte concentration, the more sensitive the electrokinetic characteristics of the porous layers to the spatial details of the distribution of the gel concentration in the diffuse interface.

In many experimental studies on the electrokinetics of soft layers such as gels or polyelectrolytes,[26−29] Ohshima's theory largely overestimates the data obtained at relatively low electrolyte concentration. On the basis of the present analysis, an explanation for such discrepancies is provided. The assumption of a discontinuous distribution of the charged polymer segments in the porous layers becomes critical and requires modification when counterions are distributed over distances comparable with the characteristic length(s) pertaining to the spatial distribution of ϕ across the interface. Rigorous theoretical interpretation of electrokinetic measurements should therefore systematically start with a scrupulous analysis of the spatial functionality of ϕ (which depends on the electrolyte concentration, as revealed by swelling measurements performed on gels[28,45]) by means of tools commonly used in computational polymer chemistry (mean-field calculations, molecular dynamic simulations, etc.). Pertinent experimental investigations (spectroscopic or imaging techniques) which would provide useful complementary information are still scarce.

The theory described is to be further improved by the inclusion of more realistic spatial distributions for ϕ, as emerging from the preamble analysis of the layer structure, nonlinear relationships between friction coefficient and polymer density (relevant for dense charged layers), and computation of the electrostatics on the basis of the nonlinearized Poisson−Boltzmann equation.[40] Such extensions will be discussed in later communications.

Acknowledgment. The work was performed within the framework of the project BIOSPEC, funded by the European Commission (Contract Number EVK1-CT-2001-00086). Discussions on elements of BIOSPEC with Dr. Lee Yezek initiated this work.

LA0400508

(45) Coleman, D. L.; Gregonis, D. E.; Andrade, J. D. *J. Biomed. Mater. Res.* **1982**, *16*, 381.